Optimal transport of active particles induced by substrate concentration oscillations

J. D. Torrenegra-Rico,* A. Arango-Restrepo,† and J. M. Rubi‡
Departament de Física de la Matèria Condensada, Facultat de Física, Universitat de Barcelona, Avinguda Diagonal 647, 08028 Barcelona, Spain

(Received 7 March 2023; accepted 27 June 2023; published 28 July 2023)

We show the existence of a stochastic resonant regime in the transport of active colloidal particles under confinement. The periodic addition of substrate to the system causes the spectral amplification to exhibit a maximum for an optimal noise level value. The consequence of this is that particles can travel longer distances with lower fuel consumption. The stochastic resonance phenomenon found allows the identification of optimal scenarios for the transport of active particles, enabling them to reach regions that are otherwise difficult to access, and may therefore find applications in transport in cell membranes and tissues for medical treatments and soil remediation.

DOI: 10.1103/PhysRevE.108.014134

I. INTRODUCTION

The autonomous movement of active particles (APs) generated by the consumption of energy from the environment gives rise to transport and self-organization processes significantly different from those that occur when the particles are not active. The study of such processes and the possibility of their control is of great current interest because of their enormous casuistry in biology and physico-chemistry [1–6].

The substrate (fuel) consumed by the particles is generally unevenly distributed and its concentration decreases with time, thus altering the composition of the particle environment. A usual approximation of the proposed active particle models is to assume that the fuel concentration is almost constant along the particle trajectories, so that the driving force exerted by the catalytic reaction is constant. Such an approximation is justified when the substrate diffusion time is much shorter than the particle travel time, so that the particles always move in a homogeneous medium [7–9]. When this condition is not fulfilled, the study requires consideration of the coupled dynamics of the particles and the substrate [10–14]. Cases in which this should be taken into account include nanoparticles that use specific substrates in tissues to become activated and move to be detected in cellular diagnostic methods and bacteria that consume hazardous chemicals inhomogeneously distributed in soil and water [15–25].

Substrate dynamics is important for understanding the movement of APs in biological and porous media where in some cases it exhibits oscillatory behavior [12,26]. In such media, particles often move through irregularly shaped channels [27,28]. Such irregularities lead to entropy variations along the media that have been modeled by entropic barriers [29,30]. Application of a periodic external stimulus on particles can, in the presence of entropic barriers, lead to stochastic resonance in which the signal-to-noise ratio or spectral amplification reaches maximum values for an optimal noise level. Such a resonance is known as entropic stochastic resonance [31–37].

The coupling of particle dynamics with substrate dynamics raises the question of whether there exist optimal conditions for APs transport to take place with maximum efficiency, i.e., longer particle displacement with lower energy consumption [18,25]. Identifying scenarios in which these conditions are met is the primary objective of this article.

We will show how a periodic injection of the substrate into a confined system, characterized by an entropic potential, results in a significant increase in the spectral amplification indicating a minimization of the random effect of thermal fluctuations [38]. The cooperation between signal (substrate oscillations) and noise, characteristic of systems with stochastic resonance, facilitates the transport of particles that can travel longer distances with lower substrate consumption. The general nature of the mechanism proposed makes it applicable to a wide range of systems, such as microfluidic devices, cell membrane transporters, drug delivery, and soil remediation, to name a few. The implementation of oscillating fuel gradients in microfluidic devices, in order to study the adaptability of the active particles to the medium, has been studied in [39–42]. Such studies reveal the possibility of experimental verification of our results.

The paper is organized as follows. In Sec. II, we present the model for the transport of active particles under chemokinetic and diffusiophoretic forces in a confined medium. In Sec. III, we analyze the Langeving and Fick-Jacobs dynamics. In Sec. IV, we present our results. We demonstrate the existence of a stochastic resonance regime in which particle transport is more efficient. Finally, in Sec. IV we present our main conclusions.

II. ACTIVE PARTICLE TRANSPORT IN A CONFINED MEDIUM

We consider a set of non-interacting active particles swimming in the confined space of Fig. 1. Each particle is subjected

*jdtorrenegrar@ub.edu; jdtorrenegrar@unal.edu.co
†aarangor@unal.edu.co
‡mrubi@ub.edu; mglrb2@gmail.com

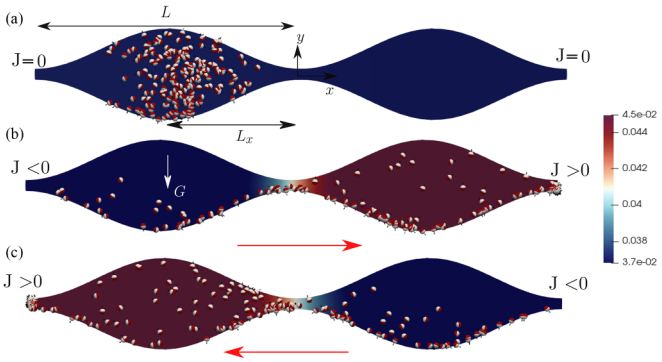

FIG. 1. Scheme of the system. The channel shape is defined in Eq. (3) in which the values of the geometrical parameters are $L_x = 1$ and $L = 2$ (both scaled with L_x). APs are driven by a constant force (white arrow) G in the orthogonal direction and by the substrate concentration gradient (color map) $\rho(x, y, t)$ in the longitudinal direction whose flux is J. The higher concentration values in the color map correspond to the red regions while the lower concentration values correspond to the blue region. Snapshots of the process: (a) initial state $t = 0$; (b) $t_1 > 0$, particles moving to the right well; (c) $t_2 > t_1$, particles moving to the left well.

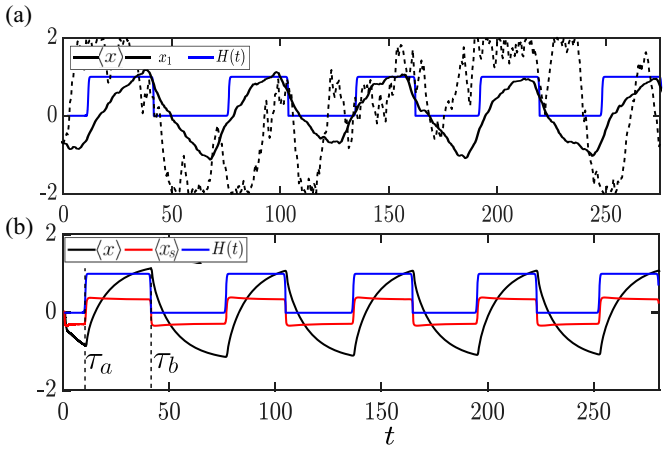

FIG. 2. Active particle dynamics. APs mean position $\langle x(t) \rangle$ (black solid line) and periodic signal $H(t)$ (blue solid line) (a) position of a single AP $x_i(t)$ (black dashed line), obtained from Langevin dynamics. (b) Substrate mean position $\langle x_s(t) \rangle$ (red line). The oscillation period is $T = \tau_b - \tau_a$ while the frequency IS $\omega = \pi/T$. The values of the parameters used in the simulations are $J_{in} = 3.25D$, $G = 1.0$, $\omega = 0.114$, $k_d = 5$, and $k_{ch} = 10$.

to a diffusiophoretic force

$$\mathbf{F}^d = k_d \nabla \rho(\mathbf{x}, t), \tag{1}$$

where $\rho(\mathbf{x}, t)$ is the substrate concentration and k_d the diffusiophoresis coefficient [9,14,43], and to a self-propelling chemo-kinetic force due to the chemical reaction taking place over the catalytic part of the particle

$$\mathbf{F}^{ch} = k_{ch} \mathcal{J}(\mathbf{x}, t)\mathbf{n}, \tag{2}$$

where k_{ch} is the chemo-kinetic coefficient and $\mathcal{J}(\mathbf{x}, t)$ the reaction flux at the particle position. We will assume that $\mathcal{J}(\mathbf{x}, t) = k_r \rho(\mathbf{x}, t)$, with k_r the reaction rate [9,14]. This force parallel to the director vector $\mathbf{n}$ has its origin in the propulsive force exerted by the bubbles generated in the catalytic part of the particle, as a product of the reaction.

The Langevin dynamics of the APs position is described by means of the Langevin equation

$$\xi_t \frac{d\mathbf{x}}{dt} = \mathbf{F}^{ch} + \mathbf{F}^d + \mathbf{F}^r, \tag{3}$$

where $\xi_t = 6\pi\mu a_p$ is the translational friction coefficient, with μ the viscosity and a_p the radius of the particles. The random term $\mathbf{F}^r$ fulfils a fluctuation-dissipation theorem [29]. Analogously, for the particle orientation ($\mathbf{n}$) we have

$$\frac{d\mathbf{n}}{dt} = (\mathbf{I} - \mathbf{nn}) \cdot \frac{1}{\xi_r} \frac{\partial \psi}{\partial \mathbf{n}} + \frac{1}{\xi_r} \mathbf{T}^r \times \mathbf{n}. \tag{4}$$

Here, $\xi_r = 8\pi\mu a_p^3$ is the rotational friction coefficient, ψ is the potential associated with the local substrate concentration gradient [14,44], and $\mathbf{T}_i^r$ is a random torque which fulfills a fluctuation-dissipation theorem. The reaction-diffusion equation for the fuel concentration is

$$\frac{\partial}{\partial t} \rho(\mathbf{r}, t) = D_s \nabla^2 \rho(\mathbf{r}, t) + \sum_{i=1}^{n} \mathcal{J}_i \delta(\mathbf{r} - \mathbf{x}), \tag{5}$$

where n is the number of particles and D_s is the diffusivity of the fuel.

The region in which active particles move is a two-dimensional compartment cell of length $2L = 40\,\mu m$ (see Fig. 1) and height

$$h(x, t) = a\left(b - \cos\left(\pi \frac{x}{L_x}\right)\right), \tag{6}$$

where $a = 15.75\,\mu$m, $L_x = 10\,\mu$m, and $b = 1.2$, from which the corresponding bottleneck diameter is 6 μm. Boundary conditions of Eq. (5) are given by

$$\frac{\partial}{\partial y} \rho \Big|_{y=\pm h(x,t)} = 0; -D_s \frac{\partial}{\partial x} \rho \Big|_{x=\pm L} = \pm J(t), \tag{7}$$

where $J(t) = J(2H(t) - 1)$. Here, J is the substrate flux at the boundaries, and $H(t) = \Theta(t - 2n\tau_a) - \Theta(t - 2n\tau_b)$, with Θ the Heaviside function, τ_a and τ_b define the period of one pulse [blue solid line on Fig. 2], and $n = (1, 2, \ldots)$. Whit these oscillation boundary conditions we ensure the oscillations of the APs and avoid the accumulation of fuel only on one side of the channel.

The cell is narrow enough for transport to occur mainly in the axial direction, with the particle distribution reaching local equilibrium very quickly in the transverse direction. This coarse-graining description, known as the Fick-Jacobs approach, in which the channel ripples are likened to entropic barriers [29–31,33–35]. The coupled particles-substrate dynamics is under this approximation described in terms of the 1d concentration and probability density, $c(x, t)$ and $P(x, t)$, defined by: $\rho(x, y, t) = c(x, t)g_s(y|x)$ and $\mathrm{p}(x, y, t) = \mathrm{P}(x, t)g_p(y|x)$ with [30,36,45]

$$g_i(x|y) = \frac{e^{-\beta U_i(x,y)}}{e^{-\beta A_i(x)}}, \quad e^{-\beta \mathcal{A}_i(x)} = \int e^{-\beta U_i(x,y)} dy, \tag{8}$$

where $i = (s, p)$, $\beta = (k_B T)^{-1}$, with k_B the Boltzmann's constant and T the temperature, $U_i(x, y)$ the potential, and $\mathcal{A}_i(x)$ the free energy of mean force of APs and fuel.

Our analysis will be performed in terms of the dimensionless quantities $\hat{x} = x/L_x$, $\hat{c}(x,t) = c(x,t)/c_0$, with c_0 a reference concentration (1D), and $\hat{\rho}(\mathbf{r},t) = \rho(\mathbf{r},t)/\rho_0$, with ρ_0 a reference concentration (2D) the reference force $F_R = \xi_R L_x^2/(k_B T)$, where $k_B T$ is the Boltzmann term and ξ^R is the reference friction coefficient, which depends on AP reference radius a_R. The relative diffusivity of the particle is defined as $\hat{D} = a_R/a_p$, and the relative diffusion of the substrate as $\hat{D}_s = \hat{D}(a_R/a_s)$. The ratio between AP reference radius and substrate radius is set as $(a_R/a_s) = 100$. The dimensionless time is $\hat{t} = t/\tau_d$, with $\tau_d = L_x^2/\hat{D}$. For convenience, we rewrite $\hat{k}_d = k_d/\hat{D}$ and $\hat{k}_{ch} = k_{ch}/\hat{D}$ then we define the dimensionless diffusiophoretic constant as $\hat{k}_d = k_d c_0/(k_B T)$, the chemo-kinetic constant as $\hat{k}_{ch} = k_{ch} c_0/(\xi_R L_x)$ and the reaction rate $\hat{k}_r = k_r \tau_d$. From now on, we will omit the tilde symbols.

In the coarse-graining description, the fuel concentration evolves according to the reaction-diffusion equation

$$\frac{\partial}{\partial t} c(x,t) = \frac{\partial}{\partial x}\left(D_s \frac{\partial}{\partial x} + D_s \frac{\partial \mathcal{A}_s}{\partial x} \right) c(x,t) + \mathcal{J}\mathrm{P}(x,t), \quad (9)$$

where the drift force is an entropic force due to the irregular shape of the boundary deriving from the entropic potential $\mathcal{A}_s = -2\ln(h(x))$. The effective reaction flux in this description is $\mathcal{J} = -k_r c(x,t)$.

In the overdamped regime, the probability distribution of the particles evolves according to the Fick-Jacobs equation

$$\frac{\partial}{\partial t}\mathrm{P} = \frac{\partial}{\partial x}\left[D\frac{\partial}{\partial x} + \frac{\partial \mathcal{A}_p}{\partial x} + \mathrm{F}_d + \mathrm{F}_{ch} \right] \mathrm{P}, \quad (10)$$

where the entropic potential is $\mathcal{A}_p = -D\ln[\frac{2D}{G}\sinh(\frac{Gh(x)}{D})]$, with G a dimensionless transverse force applied in order to fix the particles to the potential wells thus generating an activation regime [34,36]. The diffusiophoretic force is in the coarse-graining description given by $\mathrm{F}_d = k_d(\frac{\partial c(x,t)}{\partial x} - c(x,t)\frac{d\ln h(x)}{dx})$ [14]. On the other hand, the chemo-kinetic force in 1D is written as $\mathrm{F}_{ch} = -k_{ch}\mathcal{J}n$, where n is the director vector in one dimension, i.e., a scalar quantity that changes sign as a function of the difference in concentration between the two compartments of the channel: $n = \Delta c(x,t)/c_{\max}$, with $c_{\max}$ a reference value corresponding to the maximum substrate concentration.

Periodic variations of the fuel concentration in the cell are induced by bringing its ends into contact with substrate sources giving rise to the boundary conditions $\frac{\partial}{\partial x}c(x,t)|_{x=\pm L} = \pm J(2H(t)-1)$. The boundary conditions corresponding to Eq. (10) are $\frac{\partial \mathrm{P}(x,t)}{\partial x}|_{x=-L_x} = \frac{\partial \mathrm{P}(x,t)}{\partial x}|_{x=L_x} = 0$. The initial value for both $\mathrm{P}(x,t)$ and $c(x,t)$ is a δ function centered on $-L_x$ and L_x.

III. LANGEVIN AND FICK-JACOBS DYNAMICS

To solve the Langevin equations (3)–(5), we implemented a multi-scale method [46] which uses the Euler scheme for both $\mathbf{x}$ and $\mathbf{n}$ and the Crack-Nicholson finite element method for $\rho(\mathbf{r},t)$. We analyzed the evolution of a set of 200 non-interacting particles with boundary conditions that prevent them from leaving the channel [35]. To solve the Fick-Jacobs equations (9)–(10), we implemented a finite element method. Figure 2 illustrates the dynamics of the APs for the two approaches used. In the figure, we represent the average position of the particles $\langle x \rangle$ which for both approaches follows the same behavior indicating that the Fick-Jacobs method is sufficient to capture the particle dynamics and allows us to reduce the computational time. We also represent the pulse $H(t)$. In Fig. 2(a), we represent the single-particle dynamics x_i and in Fig. 2(b) the variations in substrate concentration due to the pulse effect.

Substrate injection oscillations induce periodicity of the chemo-kinetic and diffusiophoretic forces. To find the effective potential associated with the total drift on the particles [8,33], we will use the Rayleigh function [47–50]

$$\mathcal{R}(x,\dot{x},t) = \Phi(\dot{x},t) - \frac{\partial \mathcal{A}_p(x)}{\partial x}\dot{x} - (\mathbf{F}_{ch} + \mathbf{F}_d)\dot{x} \quad (11)$$

with $\dot{x}$ the velocity of the particle. The first term of this expression is the dissipation function $\Phi(\dot{x},t) = \frac{1}{2}\xi\dot{x}\dot{x}$, the second term is the free energy rate due to the entropic forces and the last term is the free energy rate related with the diffusiophoretic and chemo-kinetic forces. In the Rayleighian, we have ignored the thermal fluctuations of the substrate and the particle, since active and entropic forces dominate the process. The dissipation function is related to the minimum of the Rayleigh function $\mathcal{R}^*$ with respect to $\dot{x}$, in the form

$$\mathcal{R}^*(x,\dot{x}^*,t) = -\Phi(\dot{x}^*,t) = -\frac{1}{2\xi}\left(\frac{\partial \mathcal{A}_p(x)}{\partial x} + (\mathbf{F}_{ch} + \mathbf{F}_d) \right)^2, \quad (12)$$

in which $\dot{x}^*$ is the particle velocity path, which depends on x and t, that minimizes the Rayleigh function. In view of Eq. (12), Eq. (10), can be written as

$$\frac{\partial \mathrm{P}}{\partial t} = \frac{\partial}{\partial x}\left[D\frac{\partial}{\partial x} + \sqrt{2\xi^{-1}\Phi(x,t)} \right] \mathrm{P}, \quad (13)$$

where the drift term results from the effective potential V_{eff} defined through

$$\frac{\partial V_{\mathrm{eff}}(x,t)}{\partial x} = \sqrt{2\xi^{-1}\Phi(x,t)}. \quad (14)$$

Figure 3 shows the oscillations of the dissipation function $\Phi(x,t)$ (dashed red line) and of the effective potential $V_{\mathrm{eff}}(x)$ (solid black line), together with the variations of the AP probability $P(x,t)$ (solid black line) and the substrate concentration $c(x,t)$ (solid blue line). Parts (a,b) of the figure show that the AP probability reaches a maximum when the dissipation function is minimum. Moreover, the positive and sharp concavity of the dissipation function is related to the global maximum of P. In (b,d), we observe how the peak of the probability distribution shifts together with the concentration peak towards the ends of the channel, thus observing an almost complete passage of the particles through the bottleneck.

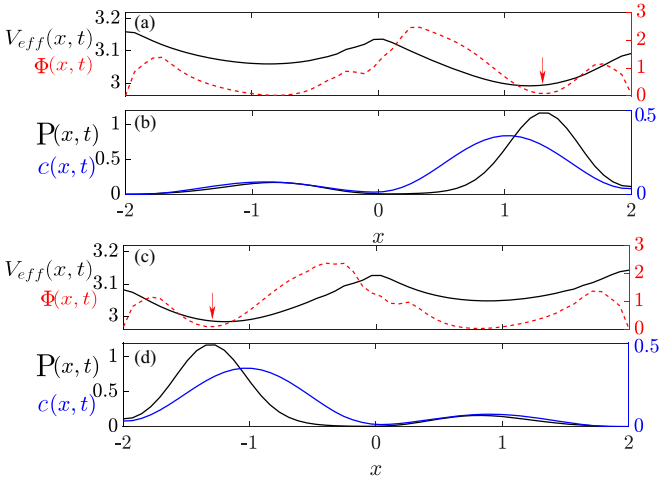

FIG. 3. Effective potential, dissipation function, particle probability, and substrate concentration at $t = 1.0$ (a),(b) and $t = 28$ (c),(d); (a),(c) Effective potential $V_{\text{eff}}(x,t)$ (black line), and dissipation function $\Phi(x,t)$ (red line); (b),(d) probability distribution (black line) and fuel concentration (blue line). The parameters used are: $J = 3.25D$ $k_r = 1$, $G = 0.15$, $\omega = 0.114$, $k_d = 5$, $k_{ch} = 10$. Red arrows indicate the location of the minimum of Φ and the maximum of the probability distribution of the active particle.

IV. RESULTS

A. Stochastic resonance regime

We have computed the spectral amplification $\eta = (M_1/F_0)^2$, where M_1 is the first harmonic of $\langle x(t)\rangle$ at long times, in Fourier space and F_0 is the input signal amplitude [34,38]. In this work, we have considered a dimensionless input signal amplitude: $F_0 = 1$, see Fig. 2 (solid blue line). For this reason, we computed the maximum distance the particles can reach $\bar{x}_{\max}$, as a function of the model parameters [35]. This quantity can be expressed as $\bar{x}_{\max} = \langle x\rangle + \sigma$, where σ is the standard deviation of x. From the substrate concentration, we have computed the substrate consumption $\mathcal{C}$

$$\mathcal{C} = \frac{1}{t_T}\int_0^{\infty}\int_{-L}^{L} \mathcal{J}\,dx dt. \tag{15}$$

where t_T is the total time.

Figure 4 shows that cooperation between periodic substrate oscillations in the cell and thermal noise leads to a maximum of the spectral amplification which results in a decrease in the substrate consumption and an increase in the maximum distance that particles reach in the cell. In Fig. 4(a), we represent the substrate consumption and the maximum distance as a function of D with and without fuel injection (squares and circles, respectively). Under fuel injection, particles reach the resonant state at $D \sim 0.3$, at which the spectral amplification represented in the inset has a maximum close to the maximum of $\bar{x}_{\max}$ at $D \sim 0.25$. Beyond this value, $\mathcal{C}$ saturates.

In our model, the presence of thermal fluctuations and the availability of substrate are key in driving particles towards the bottleneck. In the case of a closed system, without fuel supply, the substrate quickly achieves a homogeneous distribution, which does not favour particle transport. A periodic injection of substrate restores the substrate consumed by the particles

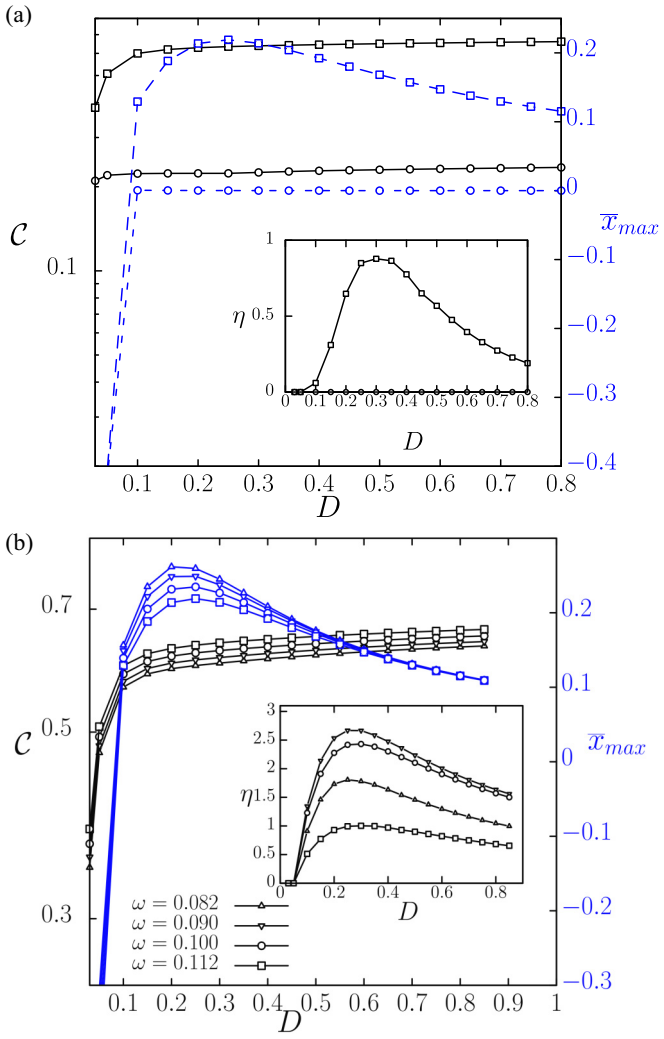

FIG. 4. Representation of $\mathcal{C}$, $\bar{x}_{\max}$ and η (inset) as a function of D. (a) With fuel injection, $J = 0.0125D_s$, (squares) and without fuel injection (circles), for $k_r = 1.0$, $k_{ch} = k_d = 5$, $G = 1$, and $\omega = 0.114$. (b) Behavior of these quantities as a function of the injection frequency, for $k_r = 1.0$, $k_{ch} = k_d = 5$, $G = 1$, and $J = 0.0125D_s$. The insets represent the spectral density as a function of the noise level.

and brings the system to the quasi-stationary state shown in Fig. 2.

Figure 4(b) shows the existence of an optimal value of the oscillation frequency of fuel supply that facilitates particle transport. The frequencies used here destroy the coherent response of the system leading to a discrepancy between the values of η and $\bar{x}_{\max}$. For $\omega = 0.082$ the value of $\bar{x}_{\max}$ is lower than that for $\omega = 0.09$, evidencing a non-monotonous behavior of the transport and consumption with the frequency. There is, therefore, an intermediate frequency that maximizes transport and minimizes consumption at a noise level value where η reaches a maximum, as shown in the box.

The noise level at which the maxima of η and $\bar{x}_{\max}$ are observed is $D \sim 0.25$, which corresponds to particle sizes $a_p = 4a_R$, at which resonant behavior is found. Using the relation a_R/a_s we find $a_p = 400a_s$. When fuel is H_2O_2, whose particle size is of about 0.25 nm, the radius of the APs is

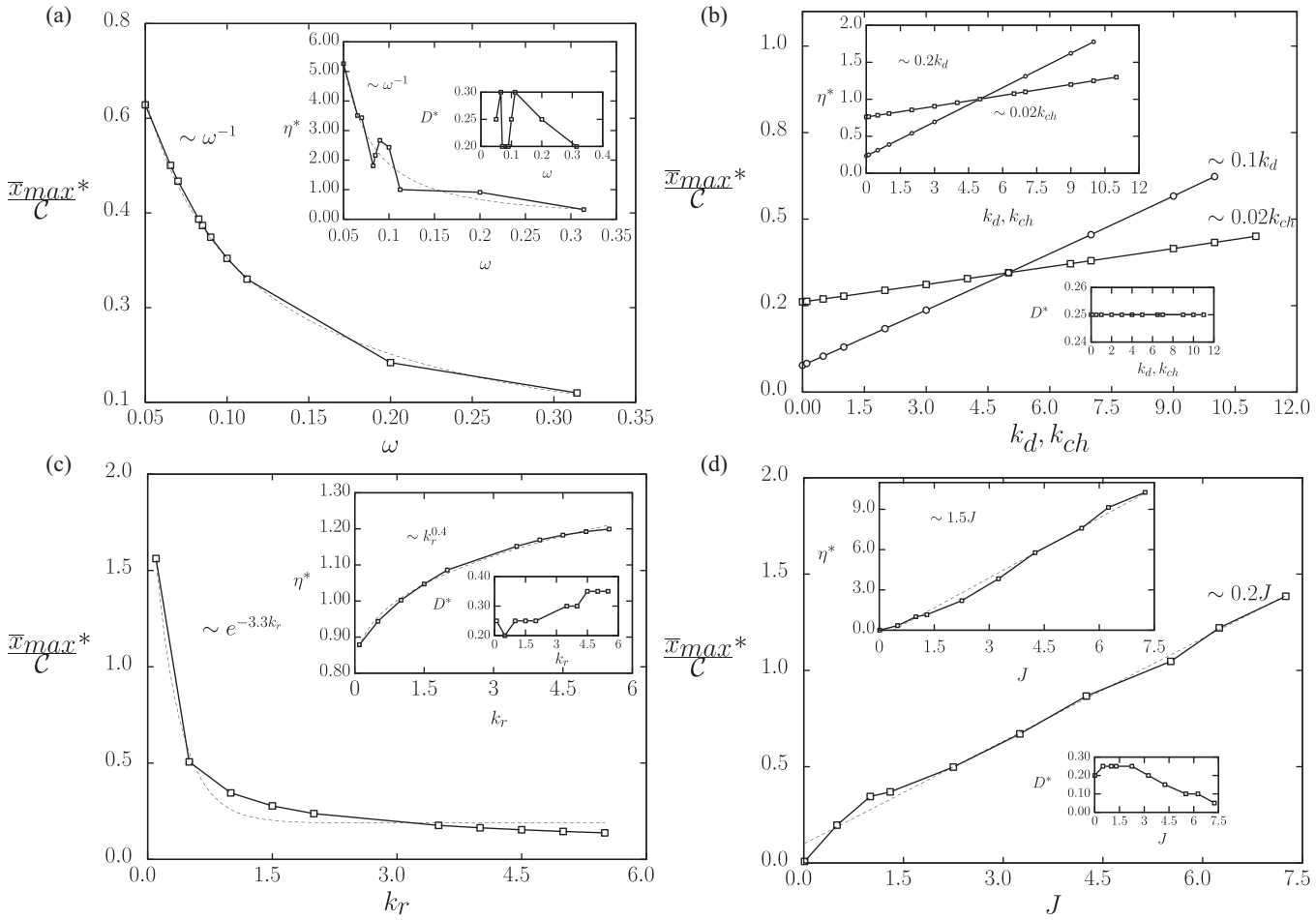

FIG. 5. Representation of the maximum distance traveled by the APs per amount of fuel consumed $\overline{x}^*_{\max}/\mathcal{C}$, the spectral amplification η^* and noise D^*at which those maximums were found as a function of (a) frequency ω, for $k_d = 5$, $k_{ch} = 5$, $G = 1$, $k_r = 1$, and $J = 1.25D$; (b) chemo-kinetic coefficient k_{ch} (lines with squares), for $k_d = 5$, and diffusiophoretic coefficient k_d (lines with circles), for $k_{ch} = 5$, both curves obtained for $\omega = 0.114$, $G = 1$, $k_r = 1$, and $J = 1.25D$; (c) reaction rate constant k_r, for $\omega = 0.114$, $k_d = 5$, $k_{ch} = 5$, and $G = 1$); and (d) substrate flux J, for $\omega = 0.114$, $k_d = 5$, $k_{ch} = 5$, $G = 1$, and $k_r = 1.0$.

$a_p = 0.1\,\mu$m, whereas if the fuel is glucose, of particle size 0.9 nm, $a_p = 0.36$ μm. The different behaviors of η and $\overline{x}_{\max}$ observed in Fig. 4 indicate that energetic efficiency and transport efficiency do not necessarily occur simultaneously.

The amount of substrate that the particles need to consume to travel a maximum distance, i.e., $\overline{x}_{\max}/\mathcal{C}$, is a measure of transport efficiency. We have computed $\overline{x}_{\max}/\mathcal{C}$ and η, and calculated the maximum values of these functions which we denote by $\overline{x}^*_{\max}/\mathcal{C}$ and η^* and represent as a function of the parameters a_p, ω, k_d, k_{ch}, k_r, and J. We have also computed the noise level D^* at which those maximum values are found.

The advantage of the periodic chemokinetic force over other periodic external forces, which could also give rise to stochastic resonance, is that the former is generated by a change of fuel concentration in the system which is easier to implement experimentally [39–41]. The latter requires the identification of a property of the particles, such as the electric charge, which may be subject to change due to their interaction with the bath. Moreover, the application of an external force could also affect the fuel concentration distribution and thus the chemokinetic forces.

B. Resonance-induced transport enhancement

In Fig. 5(a), we show that $\overline{x}^*_{\max}/\mathcal{C}$ and η^* behave approximately as ω^{-1}, which points to a reduction in efficiency as the fuel input frequency increases. We observe a non-monotonic behavior of η^* within the frequency interval $0.082 < \omega < 0.09$, which contrasts with the monotonic behavior of $\overline{x}^*_{\max}/\mathcal{C}$ which highlights the difference between transport and energy efficiencies. The resonant regime take place at $0.2 < D^* < 0.3$ for all values of ω. For frequencies $\omega \sim 0.05$, the optimal particle radius, at which the APs has resonant behavior, is four times larger than the reference radius. For example, when the substrate is H_2O_2 the radius is 0.1 μm, while when for glucose is 0.36 μm.

In Fig. 5(b), we see that $\overline{x}^*_{\max}/\mathcal{C}$ and η^* depend linearly on k_d (circle lines) and k_{ch} (square lines) for the values of the parameters indicated in the figure legend. The noise level at which the maxima occur is $D \sim 0.25$, and the particle radius is four times the reference radius. Our results show that both efficiencies are more sensitive to changes in k_d than to changes in k_{ch} if both have a value higher than 5. Suggesting that under confinement diffusiophoresis is dominant, possibly because the entropic effects over the

gradient of $c(x,t)$ in F_d are higher than the reaction flux $\mathcal{J}$ effect over F_{ch}. That makes diffusiophoresis more efficient over longer distances than chemo-kinesis, as previous results indicate [11,18,20,22].

In Fig. 5(c), shows the behavior of $\bar{x}^*_{\max}/\mathcal{C}$, η^*, and D^* as a function of k_r, whereas transport efficiency behaves exponentially, energetic efficiency follows a power law. We see that D^* increases monotonically with k_r. The maximum value reached by the energetic efficiency is found at $k_r \sim 5$ which corresponds to $D^* \sim 0.35$, and to the APs radius $a_p \sim 2.8a_R$. For $k_r \ll 1$, $D^* \sim 0.25$ and the APs radius increases: $a_p \sim 4a_R$. On the other hand, increasing k_r reduces fuel readiness which affects the diffusiophoretic and chemo-kinetic forces. This fact has not been observed in previous treatments where the fuel concentration is considered to be unchanged. In this case, variations of k_r lead to sub-optimal transport and energetic efficiencies. We can then conclude that an increased particle travel distance results in heightened fuel consumption, an undesirable outcome.

Figure 5(d) shows an almost linear dependence of $\bar{x}^*_{\max}/\mathcal{C}$ and η^* on the substrate flow J. The quantity D^* decreases for flux values between 0.05 and 0.3. As a result of those linear behaviours, increasing substrate concentration improves transport efficiency, which means an increase in distance traveled without a considerable increase in substrate consumption. Optimal efficiencies occur at $J \sim 7D_s$ which correspond to $D^* = 0.05$, and to particle sizes of about 20 times that of the reference size. As shown above, the optimal particle size depends on the type of fuel used. For H_2O_2 the size is 0.5 μm, while for glucose is 1.8 μm.

Our analysis allows us to identify the values of the model's parameters that optimize APs transport. This is the case when: $k_d = 5, k_{ch} = 15, k_r = 3, J = 3.250D, G = 1$, and $\omega = 0.114$. The noise intensity at which this maximum occurs is $D = a_R/a_p \sim 0.1$. When the substrate is H_2O_2 or glucose the radii needed to reach the optimum efficiencies fall in the range 0.015 μm–0.15 μm. The selected parameter values offer insights into the optimal particle sizes for efficient transportation. These sizes predominantly fall within the nanoscopic range, making them suitable for particles that can pass through cell membrane transporters and facilitate drug delivery in medical applications. Similar studies using auto-chemotactic droplets on irregular channels with substrate sources dependence have been carried out in [11], and are important to control and quantify the behavior of APs inside the channels.

V. CONCLUSIONS

The fuel in the bath results in a chemokinetic force on the particles. Its consumption by the particles causes their concentration to decrease, so that the displacement of the particles becomes smaller and smaller at long time limit. We have shown that oscillations in substrate concentration produced by periodic injection into a cell restores the effect of the chemo-kinetic force and result in a transport optimization in which APs need to consume less substrate to move. Intermittent injection induces a periodic force on particles whose synchronization with noise induces a stochastic entropic resonance regime in which spectral amplification is maximized and transport is optimized.

Our study enables us to identify optimal conditions for the transport of active particles, allowing them to reach regions that are difficult to access, and could therefore find applications in transport across cell membranes, drug delivery for medical treatments, and porous media.

ACKNOWLEDGMENTS

The authors are grateful for the financial support of MICIU (Spanish Government) under Grant No. PGC2018-098373-B-I00.

[1] S. J. Ebbens and J. R. Howse, Soft Matter **6**, 726 (2010).
[2] M. E. Cates and J. Tailleur, Annu. Rev. Condens. Matter Phys. **6**, 219 (2015).
[3] C. Bechinger, R. Di Leonardo, H. Löwen, C. Reichhardt, G. Volpe, and G. Volpe, Rev. Mod. Phys. **88**, 045006 (2016).
[4] M. C. Marchetti, Y. Fily, S. Henkes, A. Patch, and D. Yllanes, Curr. Opin. Colloid Interface Sci. **21**, 34 (2016).
[5] D. P. Hoogerheide, P. A. Gurnev, T. K. Rostovtseva, and S. M. Bezrukov, Biophys. J. **114**, 772 (2018).
[6] Y. Fu, H. Yu, X. Zhang, P. Malgaretti, V. Kishore, and W. Wang, Micromachines **13**, 295 (2022).
[7] J. P. Hernandez-Ortiz, C. G. Stoltz, and M. D. Graham, Phys. Rev. Lett. **95**, 204501 (2005).
[8] P. Malgaretti and H. Stark, J. Chem. Phys. **146**, 174901 (2017).
[9] H. Stark, Acc. Chem. Res. **51**, 2681 (2018).
[10] S. Saha, R. Golestanian, and S. Ramaswamy, Phy. Rev. E **89**, 062316 (2014).
[11] C. Jin, C. Krüger, and C. C. Maass, Proc. Natl. Acad. Sci. USA **114**, 5089 (2017).
[12] A. Laskar, O. E. Shklyaev, and A. Balazs, Langmuir **36**, 7124 (2020).
[13] N. Waisbord, A. Dehkharghani, and J. S. Guasto, Nat. Commun. **12**, 5949 (2021).
[14] J. Torrenegra-Rico, A. Arango-Restrepo, and J. Rubí, J. Chem. Phys. **157**, 104103 (2022).
[15] G. Pandey and R. K. Jain, Appl. Environ. Microbiol. **68**, 5789 (2002).
[16] R. M. Ford and R. W. Harvey, Adv. Water Resour. **30**, 1608 (2007).
[17] O. Felfoul, M. Mohammadi, S. Taherkhani, D. De Lanauze, Y. Zhong Xu, D. Loghin, S. Essa, S. Jancik, D. Houle, M. Lafleur *et al.*, Nat. Nanotechnol. **11**, 941 (2016).
[18] W. Gao, R. Dong, S. Thamphiwatana, J. Li, W. Gao, L. Zhang, and J. Wang, ACS Nano **9**, 117 (2015).
[19] S. K. Srivastava, G. Clergeaud, T. L. Andresen, and A. Boisen, Adv. Drug Deliv. Rev. **138**, 41 (2019).
[20] J. Li, B. E.-F. de Ávila, W. Gao, L. Zhang, and J. Wang, Sci. Robot. **2**, eaam6431 (2017).

[21] A. Ghosh, W. Xu, N. Gupta, and D. H. Gracias, Nano Today **31**, 100836 (2020).
[22] Z. Wu, Y. Chen, D. Mukasa, O. S. Pak, and W. Gao, Chem. Soc. Rev. **49**, 8088 (2020).
[23] L. Yang, X. Chen, X. Zeng, M. Radosevich, S. Ripp, J. Zhuang, and G. S. Sayler, Front. Microbiol. **10**, 2691 (2019).
[24] F. Ahmad, D. Zhu, and J. Sun, Environ. Sci. Eur. **32**, 52 (2020).
[25] C. Gao, Y. Wang, Z. Ye, Z. Lin, X. Ma, and Q. He, Adv. Mater. **33**, 2000512 (2021).
[26] X. Chen, C. Zhou, Y. Peng, Q. Wang, and W. Wang, CS Appl. Mater. Interfaces **12**, 11843 (2020).
[27] J. M. Rubí, A. Lervik, D. Bedeaux, and S. Kjelstrup, J. Chem. Phys. **146**, 185101 (2017).
[28] A. Arango-Restrepo, J. M. Rubi, S. Kjelstrup, B. A. J. Angelsen, and C. de Lange Davies, Biophys. J. **120**, 5255 (2021).
[29] M. H. Jacobs, *Diffusion Processes* (Springer, Berlin, Heidelberg, 1967).
[30] R. Zwanzig, J. Phys. Chem. **96**, 3926 (1992).
[31] D. Reguera and J. M. Rubi, Phys. Rev. E **64**, 061106 (2001).
[32] C. Zeng, C. Zhang, J. Zeng, R. Liu, and H. Wang, J. Stat. Mech. (2015) P08027.
[33] J. M. Rubi, Europhys. Lett. **127**, 10001 (2019).
[34] P. S. Burada, G. Schmid, D. Reguera, M. H. Vainstein, J. M. Rubi, and P. Hänggi, Phys. Rev. Lett. **101**, 130602 (2008).
[35] J. D. Torrenegra-Rico, A. Arango-Restrepo, and J. Rubí, J. Chem. Phys. **156**, 054118 (2022).
[36] P. S. Burada, G. Schmid, D. Reguera, J. Rubi, and P. Hänggi, Eur. Phys. J. B **69**, 11 (2009).
[37] Q. Zhu, Y. Zhou, F. Marchesoni, and H. P. Zhang, Phys. Rev. Lett. **129**, 098001 (2022).
[38] L. Gammaitoni, P. Hänggi, P. Jung, and F. Marchesoni, Rev. Mod. Phys. **70**, 223 (1998).
[39] Z. Xiao, A. Nsamela, B. Garlan, and J. Simmchen, Angew. Chem., Int. Ed. **61**, e202117768 (2022).
[40] C. Lozano and C. Bechinger, Nat. Commun. **10**, 2495 (2019).
[41] M. B. Byrne, Y. Kimura, A. Kapoor, Y. He, K. S. Mattam, K. M. Hasan, L. N. Olson, F. Wang, P. J. Kenis, and C. V. Rao, PLoS ONE **9**, e85726 (2014).
[42] T. Quast, K. Zölzer, D. Guu, L. Alvarez, C. Küsters, E. Kiermaier, U. B. Kaupp, and W. Kolanus, Front. Cell Dev. Biol. **10**, 943041 (2022).
[43] P. Gaspard and R. Kapral, J. Chem. Phys. **148**, 134104 (2018).
[44] J. D. Olarte-Plata and F. Bresme, Phys. Chem. Chem. Phys. **21**, 1131 (2019).
[45] M. F. Carusela, P. Malgaretti, and J. M. Rubi, Phys. Rev. E **103**, 062102 (2021).
[46] J. Molina, J. J. de Pablo, and J. P. Hernández-Ortiz, Phys. Chem. Chem. Phys. **21**, 9362 (2019).
[47] L. Onsager, Phys. Rev. **37**, 405 (1931).
[48] M. Doi, J. Phys.: Condens. Matter **23**, 284118 (2011).
[49] S. Komura and T. Ohta, *Non-Equilibrium Soft Matter Physics* (World Scientific, Singapore, 2012).
[50] H. Wang, T. Qian, and X. Xu, Soft Matter **17**, 3634 (2021).